Inorg. Chem. **2009**, *48*, 3731−3742

Ground and Excited Electronic States of Quininone-Containing Re(I)-Based Rectangles: a Comprehensive Study of Their Preparation, Electrochemistry, and Photophysics

Dibyendu Bhattacharya,[†] Malaichamy Sathiyendiran,[†] Tzuoo-Tsair Luo,[†] Che-Hao Chang,[†] Yu-Hsiang Cheng,[‡] Ching-Yao Lin,[‡] Gene-Hsiang Lee,[§] Shie-Ming Peng,[§] and Kuang-Lieh Lu*[,†]

Institute of Chemistry, Academia Sinica, Taipei 115, Taiwan, Department of Applied Chemistry, National Chi Nan University, Nantou 545, Taiwan, and Department of Chemistry, National Taiwan University, Taipei 107, Taiwan

Received December 17, 2008

The self-assembly of two rectangular compounds [{$(CO)_3Re(\mu$-QL)$Re(CO)_3$}$_2(\mu$-bpy)$_2$] (**1**, QL = 6,7-dimethyl 1,4-dioxido-9,10-anthraquinone (QL_1); **2**, QL = 1,4-dioxido-9,10-anthraquinone (QL_2), bpy = 4,4′-bipyridine) via an orthogonal-bonding approach was achieved in high yields. Their structures were characterized by single-crystal X-ray diffraction analysis. The rectangles exhibited multielectron-redox properties. The introduction of a bridging quininone moiety made notable changes in two well-separated single-electron reductions of the bpy moiety, as compared with other 2,2′-bisbenzimidazolate (BiBzlm) or thiolate- or alkoxide-bridged rectangles, followed by quasi-reversible reduction of the quininone moiety to allow the existence of different redox states. Electrochemical assessment using cyclic voltammetry and UV−vis−NIR spectroelectrochemistry revealed reversibly accessible 0, 1−, and 2− redox states. The comproportionation constant of the successive reduction processes was $K_c = 4.18 \times 10^8$ for complex **1** and 4.08×10^8 for **2**. In spite of the high K_c values, no obvious intervalence charge transfer bands were detected in either the vis, NIR, or IR regions, suggesting very weak electronic coupling between the ligand centers in the mixed-valent intermediates. In the mixed-valent intermediate, the overlap between donor and acceptor orbitals of the two bpy ligands engendered weak electronic coupling associated with distance that exceeded van der Waals ligand/ligand distances and created a class I fully isolated, non-interacting, valence-localized situation. Furthermore, unusual ligand-to-metal-to-ligand charge-transfer (LMLCT) transitions of complexes **1** and **2** at 298 K were observed in the visible region. Molecule **2** exhibited multiple emissions from the triplet-centered π–π^* intraligand (^{3}IL), metal-to-ligand charge-transfer (^{3}MLCT) and triplet ligand−ligand charge transfer (^{3}LLCT) levels and showed biexponential decay. By contrast, in complex **1**, ^{3}IL emission was absent and only single-exponential decay was observed. These results reveal the different nature of the electronically excited states between **1** and **2**. The mechanisms of the photophysical deactivation processes in these systems can be explained in terms of the electronic characteristics of the quininone molecules and possible geometrical differences of the excited states involved. In addition, the energies, characteristics, and molecular structures of the ground and lowest triplet excited state were calculated using the density functional theory method.

Introduction

In the years following exploration of the archetypical $Ru^{III/II}$ mixed valence (MV) system by Creutz and Taube (CT), several systems have been scrutinized to determine the extent of intermetallic electron delocalization.[1,2] Few examples of ligand-centered mixed valence (LCMV) properties are known,[3] among them, neutral Re(I)-based molecular rectangles, containing well-defined bipyridyl centered LCMV may be regarded as one of the frontrunners.[4] The cavity

* To whom correspondence should be addressed. E-mail: lu@chem.sinica.edu.tw. Fax: 886(2)27831237.
† Academia Sinica.
‡ National Chi Nan University.
§ National Taiwan University.

(1) (a) Creutz, C.; Taube, H. *J. Am. Chem. Soc.* **1969**, *91*, 3988. (b) Creutz, C.; Taube, H. *J. Am. Chem. Soc.* **1973**, *95*, 1086.

10.1021/ic8024099 CCC: $40.75
Published on Web 03/23/2009

dimensions of such rectangles, with doubly chelating ligands such as 2,2′-bisbenzimidazole (BiBzlm) or bridging thiolates or alkoxides, are narrow, and the LCMV intermediate state shows an intervalence charge transfer (IVCT) band.[4] The separation between the donor and acceptor orbitals of redox active linker ligands, which solely depends on the bridging ligand, falls within the van der Walls distance, thus, through-space electronic communication between ligands may be accessible, and the IVCT band has been observed in its 1− mixed valence intermediate. Although the IVCT band has been observed, the redox potential of bpy systems is highly destabilized, and stability of the mixed valence intermediates is low (comproportionation constant, $K_c = 10^3$).[4a,b] Recently, we reported the synthesis of Re(I) rectangles, in which a unique orthogonal-bonding approach was used for the preparation of the heterotopic Re(I) rectangles, and the biologically relevant quininone (QL^{2-}) moiety was introduced as a bridging ligand.[5,6] Although diruthenium(II) derivatives of mixed bpy-quininone, mixed-valence systems have been reported,[7] tetranuclear Re(I) complexes with a ligand-centered mixed valency of potentially mixed non-innocent ligand (e.g., electron rich quininone as bridging ligand and bpy as linker ligand) have not yet been addressed. In addition, the reports of bridging or linker variation on the basic structure of neutral Re(I) rectangles, which in turn affects the photophysical properties by tuning the triplet metal-to-ligand charge-transfer (^{3}MLCT), are rare in the literature.[8] Furthermore, room temperature multiple emission of Re(I) complexes still remains a challenge.[9] The choice of quininone (QL^{2-}) as a bridging ligand was prompted by the fact that the association of electron-rich systems with Re(I) results in the following: (i) stabilization of the reduction potential of the bpy system; and (ii) enhancement of the potential difference (ΔE), which is the parameter by which mixed valence stability is measured.

Herein, we report a one-pot synthesis of [{$(CO)_3$Re(μ-QL)Re$(CO)_3$}$_2$(μ-bpy)$_2$] (**1**, QL = 6,7-dimethyl 1,4-dioxido-9,10-anthraquinone (QL_1); **2**, QL = 1,4-dioxido-9,10-anthraquinone (QL_2)), and the room-temperature dual and multiple emission properties of the complexes. The ligand valence state distribution in $\mathbf{1}^n$ and $\mathbf{2}^n$, where $n = 0$, 1−, 2−, and 3− was assessed via UV−vis−NIR spectroelectrochemistry with substantial stabilization of the reduction potential of the bpy system and enhanced mixed valence stability.

Experimental Section

Materials. Reagents were used as received without further purification. The solvents used in this study were of spectroscopic grade.

Physical Measurements and Procedures. IR spectra were recorded on a Perkin-Elmer 882 FT-IR spectrophotometer. ^{1}H NMR spectra were recorded on Bruker AC 300 and AMX-400 FT-NMR spectrometers. Elemental analyses were performed using a Perkin-Elmer 2400 CHN elemental analyzer. FAB-MS data were obtained using a JMS-700 double-focusing mass spectrometer. The electronic absorption spectra were obtained on a Hewlett-Packard 8453 spectrophotometer at room temperature in a 1 cm quartz cell. Fluorescence spectra were recorded on a Hitachi F4500 spectrometer. Low temperature emission spectra were recorded using Aminco Bowmann Series 2 spectrofluorimeter. Cyclic voltammetry was carried out at a 100 mV/s scan rate in anhydrous DMF/0.2 M Bu_4NPF_6 at room temperature, using a three-electrode configuration (Pt macro disk electrodes were used as the working electrodes, platinum wire was used as counter electrode, $Ag/AgNO_3$ as a pseudoreference electrode) and a CHI 621B electrochemical analyzer under deaerated conditions. Potentials are referenced against internal ferrocene (Fc) added at the end of each experiment. UV−vis−NIR spectroclectrochemistry was performed with an airtight, optically transparent thin-layer electrochemical cell (OTTLE) constructed with a 100 mesh platinum gauze working

(2) (a) Creutz, C. *Prog. Inorg. Chem.* **1983**, *30*, 1. (b) Crutchley, R. J. *Adv. Inorg. Chem.* **1994**, *41*, 372. (c) Kaim, W.; Klein, A.; Glöckle, M. *Acc. Chem. Res.* **2000**, *33*, 755. (d) Launay, J.-P. *Chem. Soc. Rev.* **2001**, *30*, 386. (e) Ward, M. D.; McCleverty, J. A. *J. Chem. Soc., Dalton Trans.* **2002**, 275. (f) Kaim, W.; Sarkar, B. *Coord. Chem. Rev.* **2007**, *251*, 584. (g) Maji, S.; Sarkar, B.; Mobin, S. M.; Fiedler, J.; Urbanos, F. A.; Jimenez-Aparicio, R.; Kaim, W.; Lahiri, G. K. *Inorg. Chem.* **2008**, *47*, 5204.

(3) (a) Elliott, C. M.; Derr, D. L.; Ferrere, S.; Newton, M. D.; Liu, Y. P. *J. Am. Chem. Soc.* **1996**, *118*, 5221. (b) Sun, D. L.; Rosokha, S. V.; Lindeman, S. V.; Kochi, J. K. *J. Am. Chem. Soc.* **2003**, *125*, 15950.

(4) (a) Dinolfo, P. H.; Hupp, J. T. *J. Am. Chem. Soc.* **2004**, *126*, 16814. (b) Dinolfo, P. H.; Williams, M. E.; Stern, C. L.; Hupp, J. T. *J. Am. Chem. Soc.* **2004**, *126*, 12989. (c) Dinolfo, P. H.; Coropceanu, V.; Brédas, J.-L.; Hupp, J. T. *J. Am. Chem. Soc.* **2006**, *128*, 12592. (d) Dinolfo, P. H.; Lee, S. J.; Coropceanu, V.; Brédas, J. L.; Hupp, J. T. *Inorg. Chem.* **2005**, *44*, 5789.

(5) (a) Liao, R.-T.; Yang, W.-C.; Thanasekaran, P.; Tsai, C.-C.; Sathiyendiran, M.; Liu, Y.-H.; Rajendran, T.; Lin, H.-M.; Tseng, T.-W.; Lu, K.-L. *Chem. Commun.* **2008**, 3175. (b) Sathiyendiran, M.; Liao, R.-T.; Thanasekaran, P.; Luo, T.-T.; Venkataramanan, N. S.; Lee, G.-H.; Peng, S.-M.; Lu, K.-L. *Inorg. Chem.* **2006**, *45*, 10052. (c) Sathiyendiran, M.; Chang, C.-H.; Chuang, C.-H.; Luo, T.-T.; Wen, Y.-S.; Lu, K.-L. *Dalton Trans.* **2007**, 1872.

(6) (a) Pierpont, C. G.; Lange, C. W. *Prog. Inorg. Chem.* **1994**, *41*, 331. (b) Pierpont, C. G. *Coord. Chem. Rev.* **2001**, *95*, 216. (c) Izumi, Y.; Sawada, H.; Sakka, N.; Yamamoto, N.; Kume, T.; Katsuki, H.; Shimohama, S.; Akaike, A. *J. Neurosci. Res.* **2005**, *79*, 849. (d) da Silva, G. F. Z.; Ming, L.-J. *Angew. Chem., Int. Ed.* **2007**, *46*, 3337. (e) Solomon, E. I.; Sundaram, U. M.; Machonkin, T. E. *Chem. Rev.* **1996**, *96*, 2563. (f) Decker, H.; Schweikardt, T.; Tuczek, F. *Angew. Chem., Int. Ed.* **2006**, *45*, 4546. (g) Klabunde, T.; Eicken, C.; Sacchettini, J. C.; Krebs, B. *Nat. Struct. Biol.* **1998**, *5*, 1084. (h) Wilmot, C. M. *Biochem. Soc. Trans.* **2003**, *31*, 493. (i) Anthony, C. *Arch. Biochem. Biophys.* **2004**, *428*, 2. (j) Kunkely, H.; Vogler, A. *J. Photochem. Photobiol. A: Chem.* **2002**, *147*, 149. (k) Arcamone, F. *Med. Res. Rev.* **1984**, *4*, 153. (l) Naff, M. B.; Plowman, J.; Narayanan, V. L. In *Anthracycline Antibiotics*; El Khadem, H. S., Ed.; Academic Press: New York, 1982; p 1. (m) Young, R. C.; Ozols, R. F.; Myers, C. E. *Clin. Rev.* **1981**, *305*, 139. (n) Quinti, L.; Allen, N. S.; Edge, M.; Murphy, B. P.; Perotti, A. *J. Photochem. Photobiol. A* **2003**, *155*, 79. (o) Churchill, M. R.; Keil, K. M.; Gilmartin, B. P.; Schuster, J. J.; Keister, J. B.; Janik, T. S. *Inorg. Chem.* **2001**, *40*, 4361.

(7) (a) Maji, S.; Sarkar, B.; Mobin, S. M.; Fiedler, J.; Urbanos, F. A.; Jimenez-Aparicio, R.; Kaim, W.; Lahiri, G. K. *Inorg. Chem.* **2008**, *47*, 5204. (b) Sadler, G. G.; Gordon, N. *R. Inorg. Chim. Acta* **1991**, *180*, 271.

(8) (a) Striplin, D. R.; Crosby, G. A. *Coord. Chem. Rev.* **2001**, *211*, 163. (b) Damrauer, N. H.; Boussie, T. R.; Devenney, M.; McCusker, J. K. *J. Am. Chem. Soc.* **1997**, *119*, 8253. (c) Rajendran, T.; Manimaran, B.; Liao, R.-T.; Lin, R.-J.; Thanasekaran, P.; Lee, G.-H.; Peng, S.-M.; Liu, Y.-H.; Chang, I-Jy.; Rajagopal, S.; Lu, K.-L. *Inorg. Chem.* **2003**, *42*, 6388. (d) Rajendran, T.; Manimaran, B.; Lee, F.-Y.; Lee, G.-H.; Peng, S.-M.; Wang, C. M.; Lu, K.-L. *Inorg. Chem.* **2000**, *39*, 2016.

(9) (a) Shaw, J. R.; Schmehl, R. H. *J. Am. Chem. Soc.* **1991**, *113*, 389. (b) Kisselev, A. V. In *The Structure and Properties of Porous Materials*; Everett, D. H., Stone, F. S., Eds.; Butterworths: London, 1958; p 195. (c) Fredericks, S. M.; Luong, J. C.; Wrighton, M. S. *J. Am. Chem. Soc.* **1979**, *101*, 7415. (d) Wang, Z.; Lees, A. J. *Inorg. Chem.* **1993**, *32*, 1493. (e) Zipp, A. P.; Sacksteder, L.; Streich, J.; Cook, A.; Demas, J. N.; DeGraff, B. A. *Inorg. Chem.* **1993**, *32*, 5629.

electrode in a 1 mm quartz cell.[10] UV−vis−NIR spectra were recorded with a Jasco V-570 UV−vis−NIR Spectrophotometer. Both electrolysis cells were assembled under an inert atmosphere in a glovebox equipped with drytrain to exclude moisture and oxygen.

Excited-State Lifetime Measurements. Excited-state lifetimes of rectangles **1** and **2** were measured using a time-resolved laser spectrometer constructed in-house. The instrument was equipped with a Quanta Ray GCR-170, pulsed Nd:YAG laser. The third harmonic of the laser (355 nm, fwhm = 10 ns) was used as the excitation source. Emission signals were focused into an ARC SpectraPro-500 double monochromator. The monochromator output was sent to a PMT (Hamamatsu, R928). The signal was digitized using a LeCory 9350A digitizer. Single and biexponential decays were observed in **1** and **2**, respectively, and the lifetimes obtained were found to be reproducible within 5%.

Synthesis of [{(CO)$_3$Re(μ-QL$_1$)Re(CO)$_3$}$_2$(μ-bpy)$_2$] (1). The reaction of a mixture of $Re_2(CO)_{10}$ (147.5 mg, 0.103 mmol), 4,4′-bipyridine (35.6 mg, 0.103 mmol), and H_2QL_1 (52.7 mg, 0.10 mmol) in 12 mL of toluene was carried out in a Teflon-lined stainless steel bomb at 160 °C for 48 h. The solution was decanted, and the purple crystals of **1** were washed with hexane several times and then dried. The crystals were of X-ray quality and were characterized spectroscopically. Yield: 79% (321.2 mg, 0.16 mmol). IR (THF): νCO 2008 (s), 2002 (s), 1894 (s), 1888 (vs) cm^{-1}. ^{1}H NMR (400 MHz, DMSO-d_6): 8.71 (d, 8H, J = 7.2 Hz, H^1, bpy), 7.83 (d, 8H, J = 4.5 Hz, H^2, bpy), 8.32 (m, 4H, H^3, quininone), 7.88 (m, 4H, H^4, quininone), 2.2 (s, 12H, br, H^5, methyl-quininone). FAB-MS: m/z 1925.81 (M$^+$). Anal. Calcd for $C_{78}H_{52}N_4O_{20}Re_4$: C, 44.40; H, 2.48; N, 2.66. Found: C, 44.48; H, 2.33; N, 2.67.

Synthesis of [{(CO)$_3$Re(μ-QL$_2$)Re(CO)$_3$}$_2\mu$-bpy)$_2$] (2). Dark red rectangle **2** was obtained using a procedure similar to that for **1**, except H_2QL_2 was used instead of H_2QL_1. Yield: 74% (303.3 mg, 0.16 mmol). IR: νCO 2019 (s), 1915 (vs), 1892 (vs) cm^{-1}. ^{1}H NMR (400 MHz, DMF-d_6): 8.31 (d, 8H, J = 6.6 Hz, H^1, bpy), 8.02 (d, 8H, J = 6.6 Hz, H^2, bpy), 8.53 (m, 4H, H^3, quininone), 7.93 (m, 4H, H^4, quininone), 7.89 (m, 2H, H^5, quininone), 8.50 (m, 2H, H^5, quininone). FAB-MS: m/z 1869.71 (M$^+$). Anal. Calcd for $C_{67}H_{36}N_4O_{20}Re_4$: C, 41.02; H, 1.85; N, 2.86 Found: C, 41.49; H, 2.26; N, 2.63.

Crystallographic Determination. Suitable single crystals of **1** and **2** were mounted on the tip of glass fibers with dimensions of 0.20 × 0.10 × 0.10 and 0.23 × 0.18 × 0.10 mm^3, respectively and placed onto the goniometer head for indexing and intensity data collection using a Nonius KappaCCD diffractometer equipped with graphite monochromatized Mo Kα radiation (λ = 0.71073 Å). Empirical absorptions were applied using the multiscan method. Both structures were solved by direct methods, and refined against F^2 by the full-matrix least-squares technique using the WINGX,[11] PLATON,[12] and SHELX[13] software packages. Because of the disordered syndrome of guest molecules, the carbon atoms of the toluene molecules in **1** were refined isotropically. Other non-hydrogen atoms were refined anisotropically,and all hydrogen atoms were calculated and refined as riding models. Basic information pertaining to crystal parameters and structure refinement is summarized in Supporting Information, Table S1, selected bond distances are provided in Table 4.

Computational Section. The singlet ground state and singly reduced geometries of rectangles **1** and **2** were carried out in the gas phase using the B3LYP[14] functional of the Gaussion *03*[15] program package. The initial geometry was obtained from the crystal structures of **1** and **2**. The Stuttgart-Dresden (SDD) ECP[16] was used for the Re core potentials. The {(8s7p6d)/[6s5p3d]}-GTO was applied to the valence shell of Re together with the all electron 6-311G* basis set[17] for O, N, C, and H atoms. The optimized geometries of the complexes are listed in Table 4 and in Supporting Information, Figure S1 and Table S3. The lowest-lying triplet-state geometries of **1** and **2** were calculated in the gas phase using the unrestricted Kohn−Sham formalism (UKS) with the unrestricted B3LYP functional (UB3LYP). Geometry optimizations were performed without any constraints, and the optimized minima of these complexes were confirmed by harmonic vibration frequency analysis, in which no imaginary frequencies were at the energy minima. To accurately perform the UV−vis spectral analysis for vertical excitations from the ground state, computations using the time dependent density functional theory (TDDFT) in the gas phase, the B3LYP approach, and the SDD/6-311G** basis set were used in the first step. The lowest 65 singlet excited states were considered in the TDDFT calculations. Finally, to clearly depict the details of the frontier molecular orbitals, the stereocontour graphs of some related frontier molecular orbitals of the complexes for the ground states and triplet excited states were drawn with the GView 3.09 program based on the computed results. For the orbital contribution, additional single-point energy calculations were performed on the gas-phase-optimized geometries using the same method and basis set, and the molecular orbital compositions were analyzed using the AOMIX program.[18] Geometry optimizations were not attempted in the solvents because the complexes examined in the present study are very large molecules, for which optimizations in the absence of surroundings are difficult to achieve. This is especially true for the triplet states, for which the loose optimization criterion has generally been used.

(10) Lin, C.-Y.; McGlashen, M. L.; Hu, S.; Shim, Y. K.; Smith, K. M.; Spiro, T. G. *Inorg. Chim. Acta* **1996**, *252*, 179.
(11) Farrugia, L. J. *J. Appl. Crystallogr.* **1999**, *32*, 837.
(12) Spek, A. L. *J. Appl. Crystallogr.* **2003**, *36*, 7.
(13) Sheldrick, G. M. *Acta Crystallogr.* **2008**, *A64*, 112.
(14) (a) Becke, A. D. *J. Chem. Phys.* **1993**, *98*, 5648. (b) Lee, C.; Yang, W.; Parr, R. G. *Phys. Rev. B* **1988**, *37*, 785. (c) Vosko, S. H.; Wilk, L.; Nusair, M. *Can. J. Phys.* **1980**, *58*, 1200.
(15) Frisch, M. J.; Trucks, G. W.; Schlegel, H. B.; Scuseria, G. E.; Robb, M. A.; Cheeseman, J. R.; Montgomery, J. A., Jr.; Vreven, T.; Kudin, K. N.; Burant, J. C.; Millam, J. M.; Iyengar, S. S.; Tomasi, J.; Barone, V.; Mennucci, B.; Cossi, M.; Scalmani, G.; Rega, N.; Petersson, G. A.; Nakatsuji, H.; Hada, M.; Ehara, M.; Toyota, K.; Fukuda, R.; Hasegawa, J.; Ishida, M.; Nakajima, T.; Honda, Y.; Kitao, O.; Nakai, H.; Klene, M.; Li, X.; Knox, J. E.; Hratchian, H. P.; Cross, J. B.; Adamo, C.; Jaramillo, J.; Gomperts, R.; Stratmann, R. E.; Yazyev, O.; Austin, A. J.; Cammi, R.; Pomelli, C.; Ochterski, J. W.; Ayala, P. Y.; Morokuma, K.; Voth, G. A.; Salvador, P.; Dannenberg, J. J.; Zakrzewski, V. G.; Dapprich, S.; Daniels, A. D.; Strain, M. C.; Farkas, O.; Malick, D. K.; Rabuck, A. D.; Raghavachari, K.; Foresman, J. B.; Ortiz, J. V.; Cui, Q.; Baboul, A. G.; Clifford, S.; Cioslowski, J.; Stefanov, B. B.; Liu, G.; Liashenko, A.; Piskorz, P.; Komaromi, I.; Martin, R. L.; Fox, D. J.; Keith, T.; Al-Laham, M. A.; Peng, C. Y.; Nanayakkara, A.; Challacombe, M.; Gill, P. M. W.; Johnson, B.; Chen, W.; Wong, M. W.; Gonzalez, C.; Pople, J. A. *Gaussian 03*, revision B.03; Gaussian, Inc.: Pittsburgh, PA, 2003.
(16) (a) McLean, A. D.; Chandler, G. S. *J. Chem. Phys.* **1980**, *72*, 5639. (b) Krishnan, R.; Binkley, J. S.; Seeger, R.; Pople, J. A. *J. Chem. Phys.* **1980**, *72*, 650.
(17) (a) Stratmann, R. E.; Scuseria, G. E.; Frisch, M. J. *J. Chem. Phys.* **1998**, *109*, 8218. (b) Bauernschmitt, R.; Ahlrichs, R. *Chem. Phys. Lett.* **1996**, *256*, 454. (c) Casida, M. E.; Jamorski, C.; Casida, K. C.; Salahub, D. R. *J. Chem. Phys.* **1998**, *108*, 4439.
(18) (a) Schaftenaar, G.; Noordik, J. H. *J. Comput.-Aided Mol. Des.* **2002**, *14*, 123. (b) Gorelsky, S. I. *AOMIX program*; http://www.sg-chem.net/. (c) Barone, V.; Cossi, M.; Tomasi, J. *J. Comput. Chem.* **1998**, *19*, 404.

Scheme 1. Orthogonal-Bonding Approach to the Preparation of Rectangles **1** and **2**

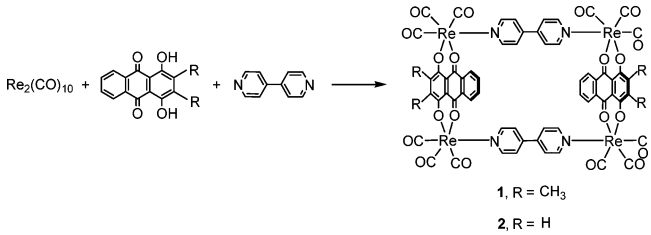

Results

Synthesis and Characterization. Synthesis of the two new molecular rectangles $[\{(CO)_3Re(\mu\text{-QL})Re(CO)_3\}_2(\mu\text{-bpy})_2]$ (**1**, QL = 6,7-dimethyl 1,4-dioxido-9,10-anthraquinone (QL_1); **2**, QL = 1,4-dioxido-9,10-anthraquinone (QL_2)) is shown in Scheme 1. The orthogonal-bonding approach,[5] which involves the simultaneous incorporation of a dianion bis-chelating ligand to coordinate two equatorial sites of the *fac*-$(CO)_3Re$ core and a neutral ditopic nitrogen-donor ligand to the remaining orthogonal axial site, was used to permit the preparation of heterotopic rectangles in high yields. The products are air and moisture-stable and are soluble in polar organic solvents.

Compared to the free ligands, ^{1}H NMR signals of bpy were shifted downfield by approximately 0.15 ppm (atom numbering for ^{1}H NMR assignment is in Supporting Information, Figure S2). The downfield shift was expected because of the formation of new coordination bonds between the nitrogen-containing ligands and the Re metal centers.[19] The IR spectrum of rectangle **2** showed bands at ~2019, 1915, and 1892 cm^{-1}, characteristic of *fac*-$Re(CO)_3$. The FAB mass spectrum of **2** showed the molecular ion peak at *m*/*z* 1869.71. The structures of complexes **1** and **2** were further confirmed by single-crystal X-ray diffraction analysis. Oak Ridge Thermal Ellipsoid Plot (ORTEP) diagrams of **1** and **2** are shown in Figure 1, and their pertinent crystallographic data can be found in the Supporting Information. The core geometry can be viewed as a molecular rectangle, in which the two $(CO)_3Rebpy\text{-}Re(CO)_3$ edges are bridged by two quininone moieties.

Structural Details. The coordination geometry around the Re centers and the bonding parameters of **1** and **2** are similar. The coordination geometry around the Re centers is a distorted octahedral with a C_3NO_2-donor environment. Each dianionic QL^{2-} ligand is coordinated through its four oxygen atoms to two Re centers in a tetradentate manner. Each 4,4′-bipyridine ligand serves as a linker that bridges two Re nodes.

The dimensions of the cavity of **1** and **2**, as defined by the Re centers, are 11.41 × 8.57 and 11.45 × 8.58 $Å^2$, respectively. However, the 4,4′-bipyridine ligands are bowed inward, such that the cavity widths of **1** and **2** at the center are reduced to approximately 7.20 and 7.60 Å, compared to 8.57 and 8.58 Å, respectively. These widths are greater than those (5.7 Å) previously reported for rectangular analogues of bpy, in which BiBzlm, rather than quininone, was used as the chelating bridging ligand.[4]

Electronic Structure. The electronic absorption spectra of the two rectangles exhibit three sets of bands in the UV and visible regions that were assigned as π-π^*, metal-to-ligand charge transfer (MLCT) transitions and ligand-to-metal-to-ligand charge-transfers (LMLCT), from electron rich $QL^{2-} \rightarrow$ bpy mixed with MLCT transitions (Figure 2 and Table 1). The fully allowed, high-energy intense band in the near-UV region (~261 nm) was assigned to the bipyridyl ligand-centered π-π^* transition as it was also observed for the free ligand. The low-energy bands (406 nm for **1** and 390 nm for **2**) in the MLCT transition were confirmed by results of the time-dependent DFT study. Notably, the MLCT band of **1** was red-shifted by 16 nm relative to **2**. However, the complex, $[\{(CO)_3Re(\mu\text{-QL})Re(CO)_3\}_2(\mu\text{-tpbb})_2]$ where QL = QL_2, and tpbb = 2,5-bis(5-tert-butyl-2-benzoxazolyl)-thiophene, showed an MLCT band at 420 nm.[5b] Absorption bands (533, 575, 625 nm for **1**; 531, 584, 632 nm for **2**) that appeared in the low-energy visible region were attributed to mixed LMLCT transitions. Assignment of this set of transitions was based on TDDFT calculations and orbital analysis (Supporting Information, Table S3 and Figure S5). Theoretical vertical excitations with oscillator strengths of **1** and **2** were consistent with the experimental results (except transition ~435−450 nm with oscillator strength > 0.6 was a failure of TDDFT for long-range charge-transfer excited states, vide infra) and can be found in Figure 2 (right).

Electrochemistry, UV−vis−NIR Spectroelectrochemistry. The redox potentials of the complexes were determined using cyclic voltammetry and are shown in Figure 3 and listed in Table 2. Reversible ligand-centered single-electron reduction occurred in the range of $E_{1/2} = -0.62$ to -1.65 V (vs Fc/Fc^+). The first two successive reduction potentials of **2** (−0.73, −1.24 V) were greater than those of **1** (−0.62, −1.13 V) when the hydrogen atom in the 6, 7-position of the parent QL_2^{2-} ligand was replaced with an electron-donating methyl substituent in QL_1^{2-}. Similarly, the shifts in the quininone reductions in **2** were more negative than those observed for **1**. The redox process at a positive potential displayed three irreversible oxidation processes for **1** and a one-step, multielectron oxidation, for **2**. After the first oxidation, a new peak was observed at −0.39 V which was absent in the first negative scan for both complexes. The appearance of the peak may be attributed to the irreversible oxidation of quininone.

In **1** and **2**, both bpy and QL^{2-} are capable of undergoing one-electron reduction; the first two bpy-based reductions are reversible, at relatively low potentials, followed by a quininone-based quasi-irreversible reduction. Second reduction of quininone is irreversible and ill-defined.[21]

(19) (a) Benkstein, K. D.; Hupp, J. T.; Stern, C. L. *J. Am. Chem. Soc.* **1998**, *120*, 12982. (b) Woessner, S. M.; Helms, J. B.; Shen, Y.; Sullivan, B. P. *Inorg. Chem.* **1998**, *37*, 5406. (c) Benkstein, K. D.; Hupp, J. T.; Stern, C. L. *Inorg. Chem.* **1998**, *37*, 5404. (d) Manimaran, B.; Thanasekaran, P.; Rajendran, T.; Lin, R. J.; Chang, I. J.; Lee, G. H.; Peng, S. M.; Rajagopal, S.; Lu, K. L. *Inorg. Chem.* **2002**, *41*, 5323. (e) Manimaran, B.; Rajendran, T.; Lu, Y. L.; Lee, G. H.; Peng, S. M.; Lu, K. L. *Eur. J. Inorg. Chem.* **2001**, 633. (f) Manimaran, B.; Rajendran, T.; Lu, Y. L.; Lee, G. H.; Peng, S. M.; Lu, K. L. *J. Chem. Soc., Dalton Trans.* **2001**, 515. (g) Dinolfo, P. H.; Hupp, J. T. *Chem. Mater.* **2001**, *13*, 3113. (h) Benkstein, K. D.; Hupp, J. T.; Stern, C. L. *Angew. Chem., Int. Ed.* **2000**, *39*, 2891.

(20) O'Boyle, N. M.; Vos, J. G. *GaussSum 1.0*; Dublin City University: Dublin, Ireland, 2005; available at http://gausssum.sourceforge.net.

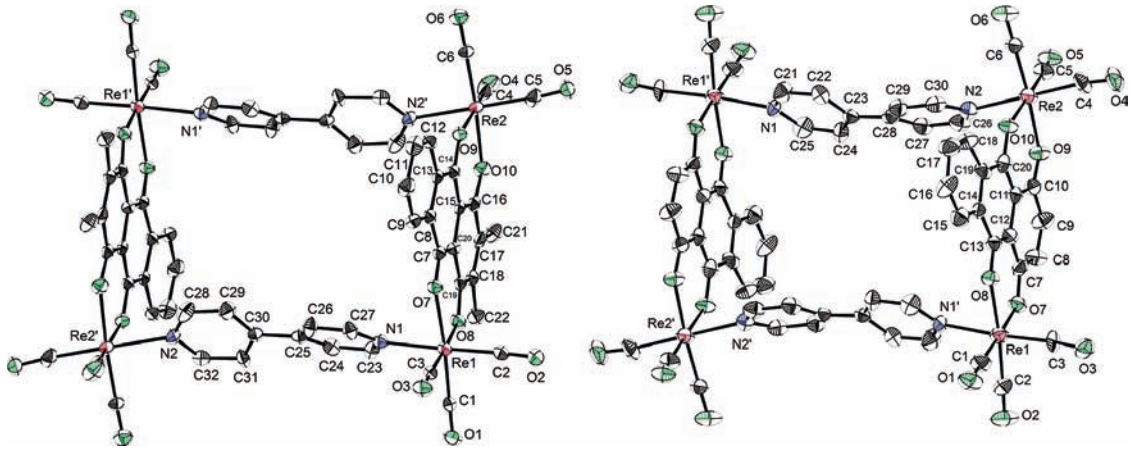

Figure 1. ORTEP diagrams of compounds **1** and **2** with atomic numbering scheme (thermal ellipsoids set at 30% probability) showing a rectangular cavity of dimensions 11.41 × 8.57 Å^2 and 11.45 × 8.58 Å^2, respectively, as defined by the metal atoms. The hydrogen atoms are omitted for clarity.

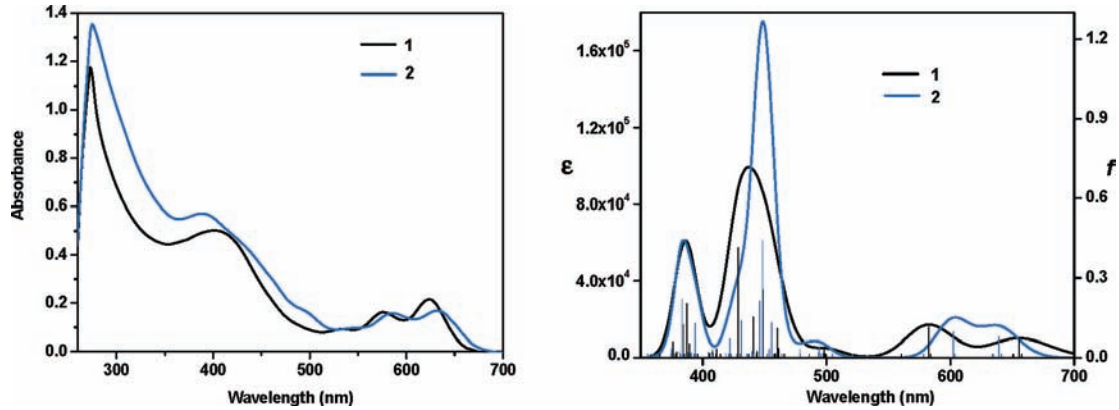

Figure 2. Electronic absorption spectra of **1** (black) and **2** (blue) in DMF (10^{-5} M) at 298 K (left). The simulated spectra with the oscillator strength (*f*) values (shown as vertical bars, same color code) were obtained with the program GaussSum 2.1.2 (right).[20]

Table 1. Electronic Absorption and Luminescence Data[a]

compound	$\lambda_{\pi-\pi^*}$, nm	λ_{MLLCT}, nm[b]	υ_{em}, × 10^3 cm^{-1} (nm)	τ, ns
1	261	406, 533, 575, 625	20.5 (489), 18.8 (533)	90
2	261	390, 531, 584, 632	23.9 (419), 22.8 (440), 20.5 (489), 19.2 (520)	19, 160
bpy	269			
QL$_1$	281	466, 483, 568	580	1.9
QL$_2$	278	471, 484, 576	577	1.2

[a] All studies were performed in Ar-saturated DMF. [b] LLCT transitions of **QL$_1$** and **QL$_2$**.

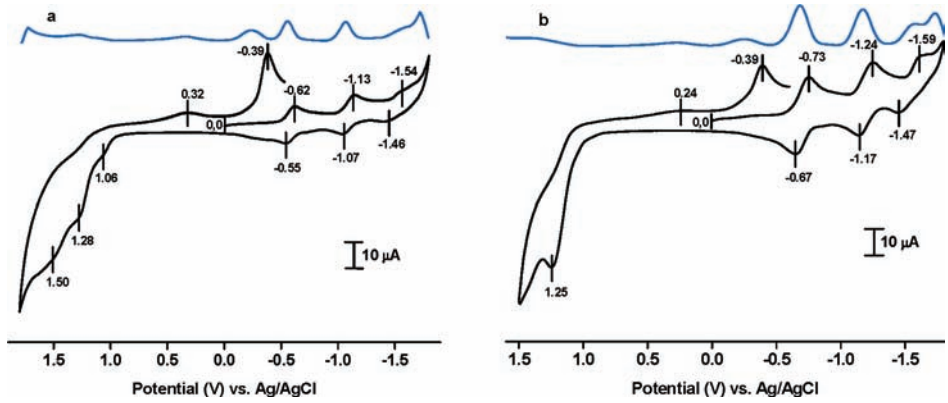

Figure 3. Cyclic voltammogram traces (black line) and Differential Pulse Voltammograms (blue line) of a 1 mM solution of (a) **1** and (b) **2** in dimethylfomamide containing 0.1 M Bu_4NPF_6 (scan rate 100 mV s^{-1}; for DPV, pulse width, 50 ms; pulse period, 200 ms; and pulse amplitude 50 mV).

Therefore, the redox reactions of **1** and **2** were investigated via UV−vis−NIR spectroelectrochemical (SEC) measurements using an optically transparent thin-layer electrochemical (OTTLE) technique to establish the likely sites of electron transfer: the accessible reductions involve 4,4′-bipyridine (and quasi-reversible 3− state for quininone ligands) for the states with $n = 0$, 1−, and 2− (Figure 4 and Table 3). Thus, the first reduction of **1** to 1− reduces the MLCT and LMCT

Table 2. Redox Potentials[a,b] and Comproportionation Constant Values (K_c)[c] for **1** and **2**

compound	$E°_{298}$ [V] (ΔE [mV])						K_c
1	−0.58 (70)	−1.09 (60)	−1.49 (80)	1.06	1.28	1.50	4.18×10^8
2	−0.70 (60)	−1.20 (70)	−1.53 (120)		1.25		4.08×10^8

[a] Potentials $E°_{298}$/V (ΔE/mV) versus Fc/Fc^+. [b] In DMF/0.1 M Bu_4NPF_6/scan rate 50 mV s^{-1}. [c] RT $\ln K_c = nF(\Delta E)$.

band intensities, accompanied by the appearance of absorption bands at about 524, and above 840 nm, which are characteristic of the radical anion form of 4,4′-bipyridine (Figure 4, Top).[22] Nearly identical behavior was observed for **2**. For both **1** and **2**, further reduction to the 2− state causes the band intensities to decrease, and most probably, a new LMLCT band is regenerated (Figure 4, middle). After the second reduction, the radical character of the bpy ligand is abolished and, as expected, the bpy^{2-} moiety did not show any characteristic band in the visible region.[22c] The presence of clean isosbestic points during each conversion and the complete electrochemical regeneration of the higher congeners without any appreciable degradation established the reversibility of the redox conversion processes under the conditions required for spectroelectrochemistry (Supporting Information, Figures S3 and S4). Further reduction to $\mathbf{1}^{3-}$ or $\mathbf{2}^{3-}$ causes a slight increase in LMLCT intensity. In this state, the electron is most likely transferred to the quininone moiety.

Emission Properties and Excited-State Lifetimes. The emission spectra for the free ligands and complexes **1** and **2** were recorded and the details are given in Table 1 and in Figure 5. Bipyridine has no detectable emission, whereas quininones displayed emission in the 580−595 nm region. Upon excitation at 390 nm, complex **1** exhibited a broad emission at about 533 nm and a shoulder around 489 nm in a room temperature solution. Similarly, compound **2** displayed a broad emission at about 520 nm and a shoulder around 489 nm. Interestingly, in addition to broad emission, complex **2** displayed a structured emission at the higher energy region of 410−440 nm.[23] Also the emission spectra of **1** and **2** were recorded at low temperature (77 K) and shown in Supporting Information, Figure S6. For complex **2** at 77 K the emission profile is more structured and displays multiple emissions with a peak at about 420 nm, due to the ^{3}IL state, and another peak at about 462 nm, due to the ^{3}MLCT state. The quantum yield of complexes **1** and **2** was calculated using $Ru(bpy)_3^{2+}$ as the standard, and it was found to be 0.157 for **1** and 0.319 for **2**. The complex **1**, upon excitation at 390 nm, exhibited single exponential decay having an excited-state lifetime of 90 ns. However, complex **2** exhibited dual exponential decay, one having a short lifetime of 19 ns (11.6%) and another with a long lifetime of 160 ns (88.4%), upon excitation at 406 nm.

Discussion

Computed Geometries and X-ray Structures. The differences between structures **1** and **2** are the Re−N and CO bond lengths. However, the bond length agrees well with that observed in analogous pyridyl-$Re(CO)_3$ rectangles.[4,19] A comparison of selected bond lengths and bond angles with computed geometries is presented in Table 4. The bond lengths and angles obtained using DFT calculations for the two complexes in the ground state were very similar (difference in bond length is less than 0.05 Å) to the experimental structure. In the series, the experimental Re−N and Re−O bond lengths were 2.217 Å and 2.094 Å for **1**, respectively.

For comparison, the theoretical values for Re−N and Re−O in compound **1** are 2.266 Å and 2.123 Å, respectively, when computed using the functional and basis set, as described above. The X-ray structures of **1** and **2** indicated that the ligands are bowed inward. The dihedral angles between the pyridine rings of bpy moiety in the rectangle are 25.28(3) and 19.79(3)° for **1** and **2**, respectively. DFT calculations of the minimum energy structure of **1** yield a dihedral angle equal to 31.87°; however, in **2** a more extreme change was observed, in which the bowed 4,4′-bipyridine ligands that were oriented inward (19.79°) became outward facing (32.15°) (Supporting Information, Figure S1 and Table S2). The twisted bpy ligand serves to minimize the separation distance at 7.5−7.8 Å, which is much longer than that required for the full van der Waals contact observed from both X-ray and geometry optimized structures. The Re−Re bond distances in these two complexes were 11.455 (long sides) and 8.575 (short sides) Å. However, rectangular Re(I) complexes with BiBZIm bridging ligands have "long" and "short" sides in lengths of 11.5 × 5.7 Å, as defined by the Re atoms.[4] Collectively, the C−O and intra-ring distances indicate that the keto−enol form of metalated QL^{2-} in both **1** and **2** is in a delocalized state. The π(Re)−π*(CO) back-bonding to the bound carbonyl lengthens the CO bond relative to free CO. The CO_{eq}–Re–CO_{eq} and CO_{ax}–Re–CO_{eq} bond angles in each ground-state complex were nearly identical, approaching 90°, which is the idealized octahedral geometry.

The repercussions of the reduction of the neutral parent precursor were evident in the dihedral angles between the pyridyl rings of the bpy moieties in each of the reduced species. These values ranged from 8.26 to 8.69° of **1** and 23.67 to 25.72° of **2** for the 1− state because of the greater degree of π overlap present in the bonds linking the pyridyl ring. The overlap in **1** was greater than that in **2**. (Supporting Information, Table S2).

Molecular Orbitals. DFT calculations indicated that the ground states of both **1** and **2** have triply degenerate highest occupied molecular orbitals (HOMOs). Compound **1** has doubly degenerate lowest unoccupied molecular orbitals (LUMOs), compound **2** has quarterly degenerate LUMOs. The 10-frontier molecular orbital energy diagram indicating the percentage orbital contribution for complexes **1** and **2** in the singlet ground state is shown in Supporting Informa-

(21) Dei, A.; Gatteschi, D.; Pardi, L. *Inorg. Chem.* **1990**, *29*, 1442.
(22) (a) Denning, M. S.; Irwin, M.; Goicoechea, J. M. *Inorg. Chem.* **2008**, *47*, 6118. (b) Braterman, P. S.; Song, J.-I. *J. Org. Chem.* **1991**, *56*, 4678. (c) Kalyanaraman, V.; Rao, C. N. R. *J. Chem. Soc. B* **1971**, 2406. (d) Roullier, L.; Laviron, E. *Electrochim. Acta* **1978**, *23*, 773. (e) Brown, O. R.; Butterfield, R. J. *Electrochim. Acta* **1982**, *27*, 321.
(23) (a) Zheng, G. Y.; Rillema, D. P. *Inorg. Chem.* **1998**, *37*, 1392. (b) Baba, A. I.; Shaw, J. R.; Simon, J. A.; Thummel, R. P.; Schmehl, R. H. *Coord. Chem. Rev.* **1998**, *171*, 43.

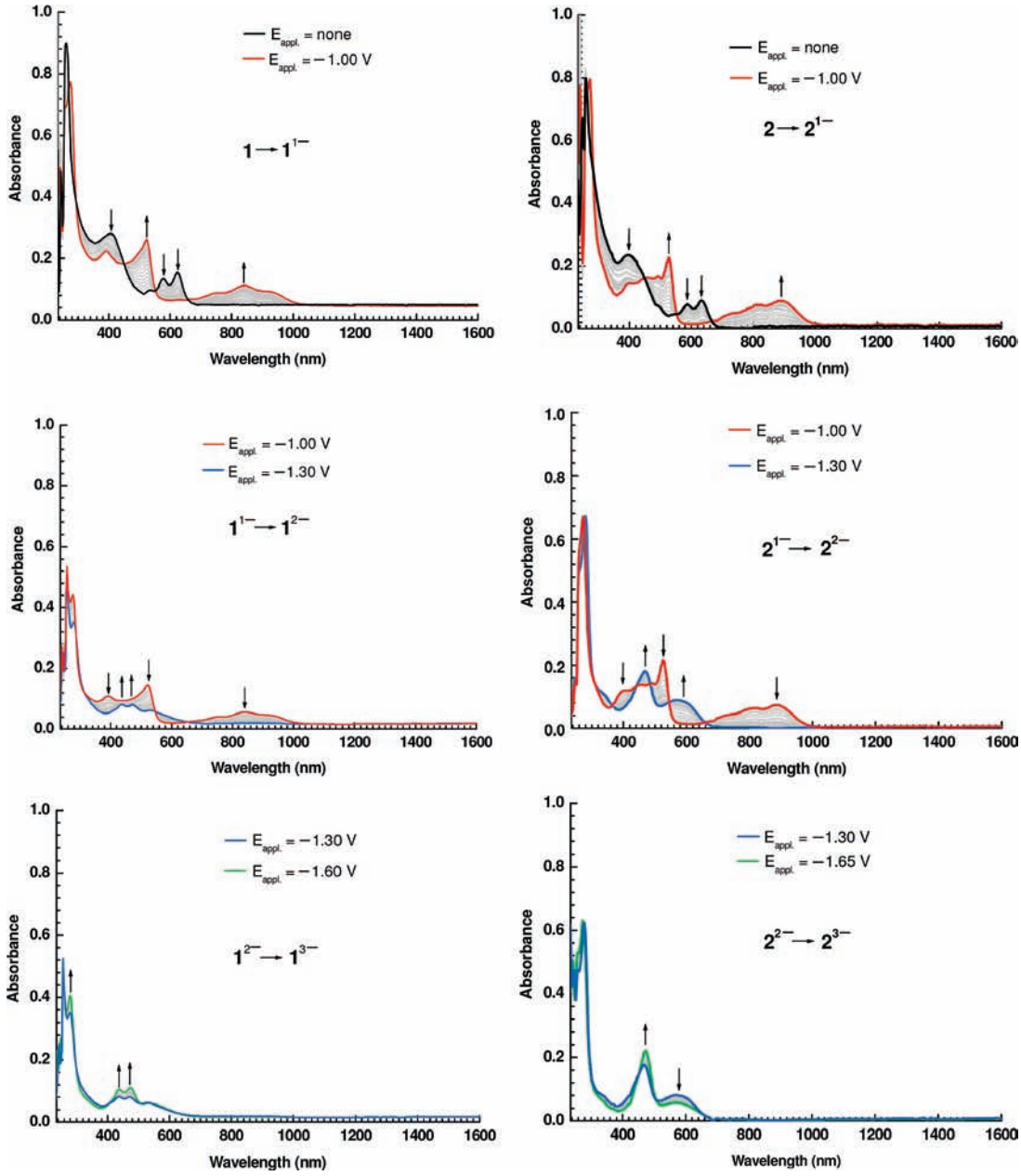

Figure 4. OTTLE spectroelectrochemistry for $\mathbf{1}^n$ and $\mathbf{2}^n$ (n = 0, 1−, 2−) in DMF/0.1 M Bu_4NPF_6. Black → red → blue → green corresponds to $\mathbf{1} \rightarrow \mathbf{1}^- \rightarrow \mathbf{1}^{2-} \rightarrow \mathbf{1}^{3-}$ conversion.

Table 3. UV-vis-NIR Data for **1** and **2** in Various Oxidation States From OTTLE Spectroelectrochemistry in DMF

compound	λ[nm] (ε [$M^{-1}cm^{-1}$])
$\mathbf{1}^{3-}$	474(131), 438(127), 278(978)
$\mathbf{1}^{2-}$	532(127), 471(160), 434(165), 280(701), 258(973)
$\mathbf{1}^{1-}$	840(113), 524(290), 392(217), 277(2313), 254(1006)
1	625(308), 575(279), 533(198), 406(563), 261(1824)
$\mathbf{2}^{3-}$	568(167), 472(496), 277(1563)
$\mathbf{2}^{2-}$	579(279), 468(553), 278(2253)
$\mathbf{2}^{1-}$	893(187), 526(446), 395(285), 275(1540), 239(1495)
2	632(520), 584(244), 531(166), 390(710), 261(2211)

tion, Figure S4. Substitution of an electron-donating methyl group in **1** destabilized the metal d orbitals. This parallels the orbital splitting between HOMO and HOMO−6. That is, the overall splitting of the Re d(t_{2g}) orbitals is greater for **1** than for **2** (0.81 and 0.77 eV, respectively), which is consistent with a greater degree of metal−ligand coupling and greater Re−N bond lengths in complex **1** compared with complex **2**. Complexes **1** and **2** have HOMO−LUMO gaps of 2.27 and 2.36 eV, respectively. The HOMOs and LUMOs of **1** and **2** closely resemble one another, and schematic diagrams of the most relevant orbitals are shown in Figure 6. Because bpy and quininone ligands are non-innocent, thus provide high-lying, filled π orbitals, the contribution of HOMO admixed to the rhenium 5d orbitals may be significant, if not dominant. The HOMO and HOMO−1 of complexes **1** and **2** (Figure 6) were ≥11% Re_d character and ≥75% quininone ligand character. However, HOMO−2 of **1** contained a π-delocalized bpy moiety, while **2** had a sizable Re_d character (79%) and 15% carbonyl character. LUMO−LUMO+3 all resulted from ligand-based π^* orbitals. The LUMO and LUMO+1 of complexes **1** and **2** contained ≥90% bpy ligand and LUMO+2 and LUMO+3 contained equivalent

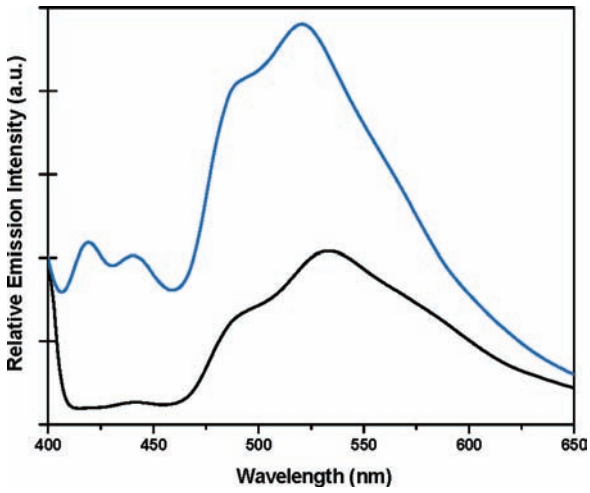

Figure 5. Emission spectra, monitored after excitation at 406 nm for **1** (black) and at 390 nm for **2** (blue) in DMF, at room temperature.

Table 4. Selected Experimental and Theoretically Calculated Bond Lengths and Bond Angles of **1** and **2**

compound	geometry	Re−N	Re−O	C−O_{ax}	C−O_{eq}	O−Re−O
		Experimental				
1	groundstate	2.217	2.094	1.176	1.154	81.8
2		2.195	2.111	1.125	1.129	82.6
		Theoretical				
1	groundstate	2.266	2.123	1.158	1.163	80.9
2		2.265	2.122	1.158	1.164	81.4
1	triplet state	2.195	2.059	1.138	1.146	83.9
2		2.255	2.130	1.157	1.163	80.5

contributions of quininones. In complex **1**, these were doubly degenerate, but in **2** all four orbitals were degenerate.

Electronic Absorption Spectra. The interpretation of the MLCT band becomes more complex when there are multiple dπ-π_1* and dπ-π_2* transitions. The Re (dπ→ quininone (πa*) and Re (dπ→ bpy (π*) transitions cannot be separated from one another, as observed for other mixed-ligand diimine complexes.[24] When two electron-donating methyl groups are attached to the same aromatic quininone ring in **1**, the MLCT band is red-shifted by 16 nm (from 390 to 406 nm). The more electron-rich quininone has a lower energy relative to the unsubstituted quininone. Singlet excited-state calculations were performed using the TDDFT method with Gaussian *03*. The results are summarized in Figure 1 (right) and Supporting Information, Table S3. Although excitation energies are slightly shifted, the intensity ratios are in good agreement with the experimental results, especially in low-energy excitation energies that show a correct position from those of experimental values.[25] The high-energy band that appeared at ∼385 nm was assigned based on TDDFT analysis to the mixed-state where the LLCT state (HOMO−12 to LUMO+3 states in **2**) is the major contributor (51%) (Supporting Information, Table S3) to the MLCT band (HOMO−3 to LUMO+8, 29%). Furthermore, the largest shift in the MLCT position was observed when the bpy ligand was replaced with the tpbb ligand, which has an electron-rich thiophene moiety. The sulfur (greater radial extension in its bonding) makes the tpbb ligand π* orbital substantially lower in energy; hence, the MLCT band shifted to 420 nm.[5b] Therefore, substitution with an electron-donating bridging ligand and/or linker with a highly electron-rich ligand causes the MLCT band to red-shift. This finding gives us a roadmap by which ligands can be selected for light harvesting materials. No solvatochromic effects were observed in the absorption spectra of **1** and **2**.

Introduction of a quininone moiety into a rectangular configuration results in additional multiple low-energy LLCT transitions with substantial MLCT character, which are rare in the literature. The enhanced absorption in the visible region as the MLCT character increases is the critical factor for light-harvesting photovoltaic cells.[26] These very low-energy bands have a profound influence on the photophysical properties required for functional optical materials. The photochemical stability of **1** and **2** in DMF solution was checked by exciting with light of 365 nm and in visible wavelengths. There is no change in the absorption and luminescence intensity after prolonged irradiation. On the basis of TDDFT calculations for **1** and **2**, these absorption bands were closely matched with the experimental results and were centered at approximately 500−650 nm, compressed by two electronic transitions with CT character. The first low-energy transition was from a mixed HOMO to the bpy while the second transition was from HOMO to quininone (LUMO+3). Both the complexes had a shoulder at 495 nm that was ascribed to a π–π* transition in **1** and a dπ Re(I)-to-π* transition in **2**. Unexpectedly, a methyl substitution in **1** caused a blue-shift in the ligand−metal−ligand charge transfer transitions (575 and 625 nm in **1** to 584 and 633 nm in **2**). As described above, π-quininone/dπ Re(I) donor to π*-acceptor orbitals are involved. Close inspection of the ligand π*-acceptor orbitals revealed substantial perturbation of tetranucleation. In addition, the extent of this orbital stabilization was related to the steric hindrance of the bridging ligand.

Electrochemical and Spectroelectrochemical Behavior. The HOMOs of complexes **1** and **2** consisted of dπ orbitals located on the metal center and of quininone ligand π orbitals. The irreversible oxidation that involves the removal of electrons from HOMOs has a sizable ligand contribution. It is difficult to quantify the number of electrons involved in such processes. Furthermore, this information is not useful, as the irreversibility of the reaction suggests that the electrogenerated species, which dissipated, was unstable in the CV time scale. One can predict that quininone normally undergoes a pair of successive two-electron oxidation.

(24) (a) Sahai, R.; Morgan, L.; Rillema, D. P. *Inorg. Chem.* **1988**, *27*, 2495. (b) Show, J. R.; Webb, R. T.; Scheml, R. H. *J. Am. Chem. Soc.* **1990**, *112*, 1117.

(25) (a) LLCT states (∼435−450 nm) have been reported as an artifact of TDDFT because of an underestimation of the energies of long-range CT. (b) Bossert, J.; Daniel, C. *Chem.—Eur. J.* **2006**, *12*, 4835. (c) Dreuw, A.; Head-Gordon, M. *J. Am. Chem. Soc.* **2004**, *126*, 4007. (d) Yamaguchi, Y.; Yokoyama, S.; Mashiko, S. *J. Chem. Phys.* **2002**, *116*, 6541.

(26) (a) Crosby, G. R. *Acc. Chem. Res.* **1975**, *8*, 221. (b) Meyer, T. J. *Acc. Chem. Res.* **1989**, *22*, 163. (c) O'Regan, B.; Grätzel, M. *Nature* **1991**, *353*, 737. (d) Gao, F.; Wang, Y.; Shi, D.; Zhang, J.; Wang, M.; Jing, X.; Humphry-Baker, R.; Wang, P.; Zakeeruddin, S. M.; Grätzel, M. *J. Am. Chem. Soc.* **2008**, *130*, 10720. (e) Chen, C. Y.; Wu, S. J.; Wu, C. G.; Chen, J. G.; Ho, K. C. *Angew. Chem., Int. Ed.* **2006**, *45*, 5822.

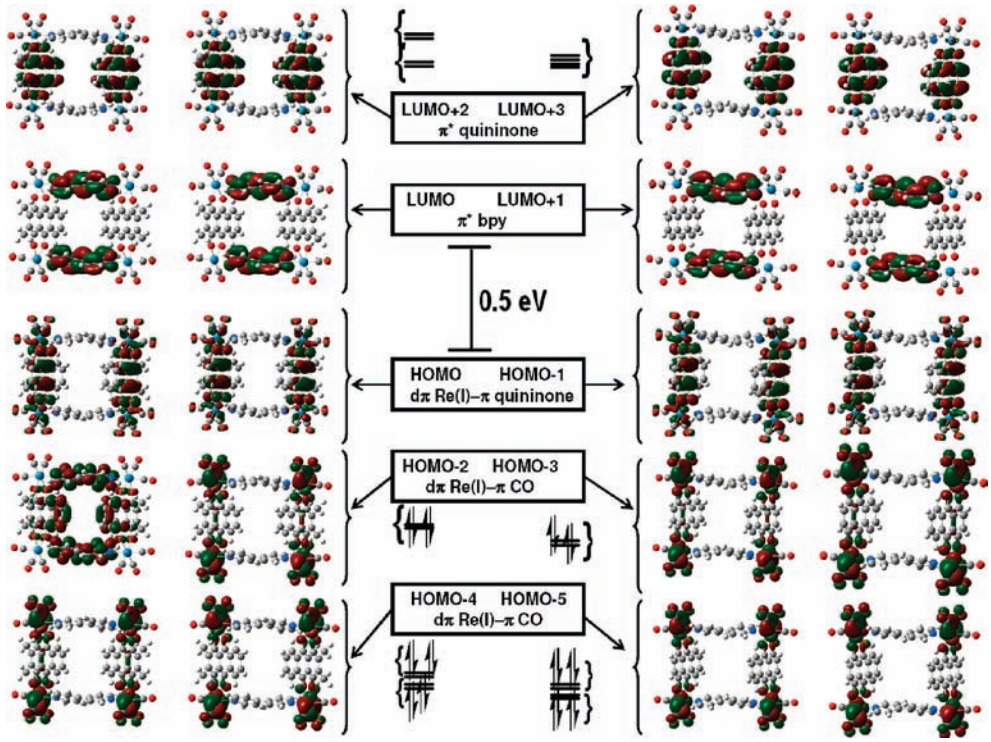

Figure 6. DFT/B3LYP/SDD molecular orbital topologies for the most relevant terms of compounds **1** (left) and **2** (right, isodensity value = 0.02). AOMIX breakdown of relevant MOs into constituent components are available as Supporting Information.[18]

Although an alternative mechanism that involves metal-centered production of a labile 17 e^- Re(II) species that undergoes facile CO substitution cannot be ruled out.[27]

The reduction process has been well-characterized as a reversible, single electron process. The first two reduction reactions involve the bpy ligand. The subsequent quininone-based reduction, which involves making an already negatively charged ligand more negative, is difficult. The electrostatic cost of adding an electron to the neutral bpy moiety is relatively low, however, as predicted from the frontier molecular orbitals. LUMO−LUMO+4 orbitals are predominantly located on both the π^* orbital of bpy and the quininone moiety with no metal contribution. In **1**, LUMO, LUMO+1, and then LUMO+2 and LUMO+3 degenerate and, as a result, have different energies. In **2**, all four orbitals have the same energy. This is the first report of quadratically degenerate orbitals in rectangular Re(I) systems.[4] It is important to mention here that the Re(I/0) metal center reduction was not observed within the solvent window.

Introduction of the quininone ring into the tetranuclear metallacycle increases the mixed valence properties of the system. As expected on the basis of the electrochemical behavior of the quininone compounds, **1** and **2** shifted to substantially more negative potentials. Lowering of the energy of the π^* orbital upon complexation with the metal stabilizes the π^* level, making the ligand resistant to reduction.[28] Addition of an electron-donating methyl group to the quininone moiety shifted the reduction potential to lower values (in the order **1** < **2**). However, extended conjugation by substituting the linker bpy with tpbb resulted in the lowest reduction potential of the quininone moiety. The formal potential differences (Table 2; Figure 3) are sufficient to permit both chemical and electrochemical preparation of solutions containing greater than 97.5% (Supporting Information, Figures S3 and S4) of each rectangle in the mono- and dianionic form. Furthermore, the low-lying, 4-fold degenerate LUMO, the doubly degenerate HOMO level, and the small energy gap between the HOMO and the LUMO (∼ 2.27 eV) make compound **2** a fairly good electron acceptor with the ability to undergo a reversible, two-electron reduction. In contrast, **1** has a doubly degenerate LUMO level and a large energy gap (∼ 2.36 eV). The facile reduction contrasts with its difficult oxidation. The third reduction, in each case, appears to be a quasi-reversible, one-electron process based on the results of cyclic voltammetry, and the electrochemical reversibility is 45%. Nevertheless, in our system, the reduction potential of bpy was substantially less than that reported for other systems. The minor changes in the composition of the bridging quininoid ligand elicit drastic changes in the bpy reduction potentials for **1** and **2**. However, in previously reported rectangles, the bridging ligand plays only a structural role.[4] Furthermore, the separation of the reduction potentials is significant, as discussed in the next section.

The primary prerequisite for molecules that are used in energy-conversion materials is multielectron redox storage capability. Potential differences are measures of mixed valence stability and of comproportionation constants of successive reduction process, K_c, ($RT \ln K_c = nF(\Delta E)$[29]) 4.18

(27) Sun, S. S.; Lees, A. J. *J. Am. Chem. Soc.* **2000**, *122*, 8956.
(28) Hartmann, H.; Berger, S.; Winter, R.; Fiedler, J.; Kaim, W. *Inorg. Chem.* **2000**, *39*, 4977.
(29) Robin, M. B.; Day, P. *Adv. Inorg. Chem. Radiochem.* **1967**, *10*, 247.

$\times 10^8$ for $\mathbf{1}^-$ and 4.08×10^8 for $\mathbf{2}^-$. The most striking result obtained using our system is the unexpectedly strong ligand center stabilization. To the best of our knowledge, such a high bpy-ligand based contribution to stability in a rhenium rectangle has not been previously reported in the literature. The only other known related complexes, incorporating a bridging BiBZIm ligand, $([Re(CO)_3]_2BiBzIm)_2$-μ,μ'-(4,4′-bpy)$_2$ and bridging thiolates or alkoxides, exhibit a K_c value of 10^3 in the respective mixed-valent state.[4] However, the K_c value of a singly reduced state Re(I) rectangle observed in our system, which was on the order of 10^8, corresponds to a moderately to strongly coupled class II system.[29] The K_c value was substantially increased by replacing the bridging π-acidic BiBzIM to the more σ-donating, electron-rich quininone.

The mixed-valency states of **1** and **2**, however, did not exhibit a clear absorption band in the near- and mid-IR regions (NIR). The crystal structure indicated that the cavity was large enough, but that the bpy ligand did not bow inward sufficiently to achieve van der Waals contact. Further geometry optimized structures of the neutral and reduced form of the rectangle indicates that the dihedral angle between pyridine rings is smaller in the reduced state. This phenomenon is greater in the case of **1**, compared with **2** (8.26° versus 31.87°, for the reduced site). A smaller dihedral angle engenders more rigidity and planarity. So, the closest possible C−C distance in the neutral form exceeds that of the reduced form (Supporting Information, Table S2). In addition, the dihedral angle change is greater in **1** than in **2**. With the BiBzlm bridging ligand,[4] the bpy dihedral angle was 39°, which was lowered to 21° in the reduced form; however, this remains within the van der Waals separation distance, and an intervalence charge transfer (IVCT) band was observed. Supporting Information, Table S2 lists the dihedral angles along with the closest possible distances (inter-ring C−C bond distance) of **1** and **2** in both the neutral and reduced forms. So, although the K_c value is high, through-space electronic communication between bpy ligands is prohibited, resulting in the valence-localized situation and full isolation. Therefore, from Hush's classical two-state theory, mixed-valent redox centers of both the compounds are considered as class I situations.[4]

Upon successive reduction, i.e., $\mathbf{1} \rightarrow \mathbf{1}^- \rightarrow \mathbf{1}^{2-} \rightarrow \mathbf{1}^{3-}$, the d$\pi$ Re(I) $\rightarrow \pi^*$ ligand MLCT transition progressively red-shifter from 408 → 389 → disappear, with a constant drop in intensity. This is probably a consequence of the sequential addition of electrons into the empty π^* orbitals of the ligand. After reduction, the energy of these orbitals is increased, and the MLCT transition shifted to a higher energy.[28] Moreover, the reduction of bpy, $\mathbf{1} \rightarrow \mathbf{1}^-$, results in the additional low-energy shoulders associated with IL transitions. Furthermore, as observed for the frontier molecular orbitals, LUMOs are degenerate, closely spaced π^* orbitals; however, various alternatives in terms of electronic transitions and orbital occupancy are possible. The intense LMLCT transition band near 600 nm in the parent complexes completely disappeared in the 1− state. Again, the MLCT band (390 nm) vanished with the concomitant growth of two new bands, which were located near 479 and above 530 nm in **1** and 470 and 579 nm in **2**. The intensity of these two new bands increased after the third reduction. The origin of these bands was probably the $QL^{3-} \rightarrow$ Re(I) or LLCT transitions. The combinations arising from this special situation are summarized in Scheme 2 (QL = QL_1 in **1** and QL_2 in **2**).

Scheme 2

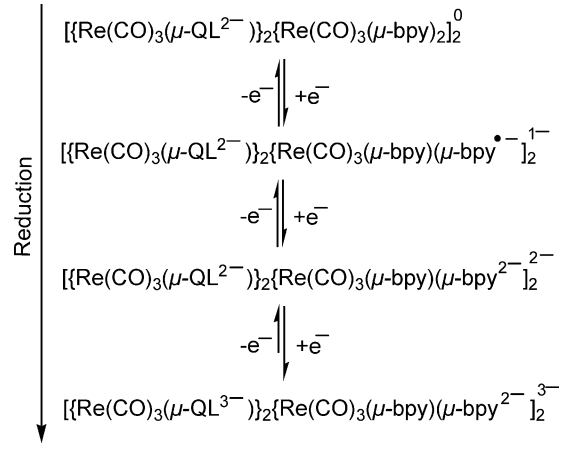

Triplet Geometry Feature and Energy. The lowest-lying triplet-state geometries of **1** and **2** were calculated using unrestricted open shell B3LYP in the gas phase. The spin contamination from states of higher multiplicity was low (⟨S⟩ was 2.0097 for **1** and 2.014 for **2**). The energies of the lowest-lying triplet states were greater than those of the corresponding ground states by 2.13 eV for **1** and by 2.41 eV for **2**. The energy difference between the two singly occupied molecular orbitals (SOMOs) was 1.15 eV in **1** and 1.09 eV in **2**. The first empty orbital was at least 0.27 eV greater than the high-energy SOMO for both complexes. The lowest-lying triplet states of **1** had substantial metal character, but in **2** the triplet state resides on the quininone moiety (Figure 7). The SOMOs do not correspond to the HOMOs and LUMOs of the ground-state geometry. The low-energy SOMO was metal, CO, and bpy based in **1**, but metal and quininone based in **2**. An attempt to obtain higher triplet excited-state energies failed; both TDDFT and Δ-SCF failed to optimize because of the large molecular size.

Emission Properties and Excited-State Lifetimes. Fluorescence from a $^1\pi$–π^* state is generally not observed in transition metal complexes.[9a] Furthermore, phosphorescence from either the ^{3}MLCT or the $^3\pi$–π^* excited state is observed because of large spin−orbit coupling exerted from the Re(I) atoms. For complex **1**, the broad emission profile suggested that the emission may be attributed to the decay of the triplet ligand−ligand charge transfer (^{3}LLCT) level at 20.5×10^3 (489 nm) and the low energy d(Re) → π^*(bpy) triplet excited state at 18.8×10^3 cm^{-1} (533 nm).[30] In contrast, compound **2** exhibited two emission profiles, a structured emission at the high-energy region and a broad emission in the low-energy region. This is further checked by recording the

(30) Song, L.-q.; Feng, J.; Wang, X.-s.; Yu, J.-h.; Hou, Y.-j.; Xie, P.-h.; Zhang, B.-w.; Xiang, J.-f.; Ai, X.-c.; Zhang, J.-p. *Inorg. Chem.* **2003**, *42*, 3393.

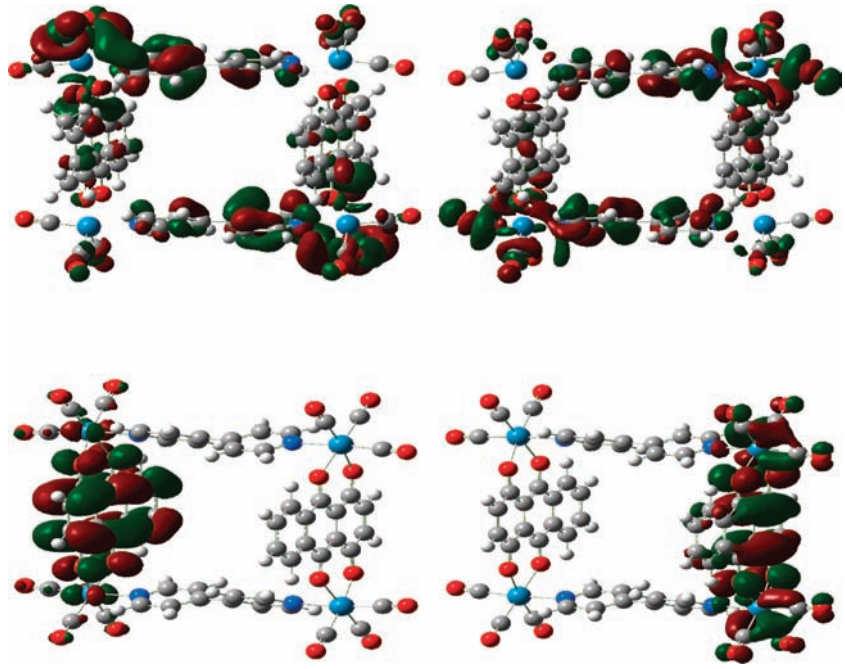

Figure 7. Molecular orbital topologies (SOMO (left) and SOMO−1 (right)) for **1** (top) and **2** (bottom) in triplet-state geometry optimized structure. (isodensity value = 0.02).

emission spectra at 77 K. The emission at about 420 nm, due to ^{3}IL state, did not show much shift in the wavelength, compared to room temperature emission spectra. The emission peak due to the ^{3}MLCT state is blue-shifted to 462 nm compared to room temperature emission that can be seen in related rhenium(I) complexes.[9c,e,23b] Also, in the excited-state lifetime profile, **2** showed biexponential decay with a short component having a lifetime of 19 ns and a long component having 160 ns. The structured emission profile and short lifetime may be attributed to the ^{3}IL excited state at the high-energy region of 23.9×10^3 (419 nm) and 22.8×10^3 cm^{-1} (440 nm) (dual emissions indicated nonthermally equilibrated ^{3}LF) and the broad emission with a long lifetime may be due to the ^{3}MLCT and ^{3}LLCT state at 20.5×10^3 (489 nm) and 19.2×10^3 cm^{-1} (520 nm).[22,31] To confirm the presence of multiple excited states, the excitation spectrum of **2** was recorded and the uncorrected excitation spectrum is shown in Supporting Information, Figure S7. The excitation spectra of **2** showed that the emission at 440 nm is indeed due to a ligand-centered transition, and the emission at 520 nm is attributed to the MLCT transition.[31]

As observed in the absorption spectra (16 nm shift in MLCT band), the second emission maxima shifted to a lower energy by 13 nm when the methyl group was attached to the quininone moiety in **1**. This is probably due to the lateral shift of the bridging quininone ring in **1**; this shift does not occur in **2**. In the lowest-lying triplet excited state, **2** has a more rigid rectangular structure than **1**. The large lateral shift in **1** indicates that the triplet excited state is constrained and more perturbed related to the ground state. This phenomenon is related to enhanced intersystem crossing (ISC), so no emission from the ^{3}LF state is observed in **1**,[32] and it also explains the shorter emission lifetime of the triplet MLCT in **1** (90 ns) as compared with **2** (160 ns). The shorter ^{3}MLCT lifetime of **1** may be attributed to the enhanced rate of non-radiative decay of **1** because of the lower energy of the excited state (2.13 eV for **1** and by 2.41 eV for **2** than those of the corresponding ground states) with a more effective vibronic overlap. Furthermore, the shape of SOMOs can help differentiate among their photophysical behaviors. As shown in Figure 7, **1** orbital had greater metal character, which was responsible for the high intersystem crossing.

Careful scrutiny of the photophysical data of the rectangle **2** reveals several interesting points. Multiple emissions involve two different phenomena: (i) the extremely short lifetime and relatively high-energy emission indicate the emission is apparently localized on non-equilibrated $^3\pi$–π^* fluorescence; and, (ii) long lifetime and low-energy emission from the ^{3}MLCT state, which is typically observed in Re(I) complexes. Enhanced mixing of the frontier orbitals of metals and ligands allows multiple emissions at room temperature in **2**, and substitution of methyl groups in quininone alters the excited-state ordering and spacing, which affects the photophysical deactivation mechanism. The emission of quininone was shifted to a higher energy when the compound was deprotonated and coordinated to the Re(I) center. This occurs because the multielectron reduction potential of quininone increased significantly upon coordination, thus lowering the emission wavelength of the ILCT transition.

Conclusion

Two new rectangular neutral Re(I) metallacycles were synthesized and investigated using spectroscopic and com-

(31) Glazer, E. C.; Magde, D.; Tor, Y. *J. Am. Chem. Soc.* **2005**, *127*, 4190.

(32) Westmoreland, T. D.; Le Bozec, H.; Murray, R. W.; Meyer, T. J. *J. Am. Chem. Soc.* **1983**, *105*, 952.

putational methods. Introduction of the electron-rich quininone bridging ligand caused unexpectedly strong ligand center stabilization and substantial changes in the potential difference between two successive reversible reduction reactions of the bpy moiety. However, the large separation between the redox-active bpy ligand does not allow through-space electronic coupling, and a non-communicating, fully valence-localized situation arises. Differences in photophysical properties help to select the appropriate ligand and therefore allow predetermination of both the lowest energy transitions and lowest emitting states in these molecules. Multiple emissions at room temperature, which are rare in the literature, were observed for **2**. The high ISC of **1** inhibits emission from the ^{3}IL state; however, intraligand phosphorescence (^{3}LLCT) and ^{3}MLCT emission were observed for both complexes.

Acknowledgment. We thank Academia Sinica and the National Science Council of Taiwan for financial support.

Supporting Information Available: X-ray crystallographic files (CIF) of **1** and **2**, geometry optimized structures of **1** and **2** in singlet, singly reduced and triplet state, dihedral angle of pyridyl group in bpy ligand and closest possible C−C contact distance, molecular orbital energies, composition and selected calculated singlet excited-state transitions for **1** and **2** in vacuum, absorbance-applied potential titration plots of **1** and **2**. This material is available free of charge via the Internet at http://pubs.acs.org.

IC8024099